J Nanopart Res (2016) 18:48
DOI 10.1007/s11051-016-3355-8

RESEARCH PAPER

A universal route for the simultaneous extraction and functionalization of cellulose nanocrystals from industrial and agricultural celluloses

Guo-Yin Chen · Hou-Yong Yu · Cai-Hong Zhang · Ying Zhou · Ju-Ming Yao

Received: 26 October 2015 / Accepted: 29 January 2016 / Published online: 11 February 2016

Abstract A simple route was designed to extract the cellulose nanocrystals (CNCs) with formate groups from industrial and agricultural celluloses like microcrystalline cellulose (MCC), viscose fiber, ginger fiber, and bamboo fiber. The effect of reaction time on the microstructure and properties of the CNCs was investigated in detail, while microstructure and properties of different CNCs were compared. The rod-like CNCs (MCC) with hundreds of nanometers in length and about 10 nm in width, nanofibrillated CNCs (ginger fiber bamboo fiber) with average width of 30 nm and the length of 1 μm, and spherical CNCs (viscose fiber) with the width of 56 nm were obtained by one-step HCOOH/HCl hydrolysis. The CNCs with improved thermal stability showed the maximum degradation temperature (T_{max}) of 368.9–388.2 °C due to the introduction of formate groups (reducibility) and the increased crystallinity. Such CNCs may be used as an effective template for the synthesis of nanohybrids or reinforcing material for high-performance nanocomposites.

Keywords Cellulose nanocrystal · Simple route · Formate groups · Thermal stability · Nanocomposites · Reinforced materials

Electronic supplementary material The online version of this article (doi:10.1007/s11051-016-3355-8) contains supplementary material, which is available to authorized users.

G.-Y. Chen · H.-Y. Yu · C.-H. Zhang
The Key Laboratory of Advanced Textile Materials and Manufacturing Technology of Ministry of Education, College of Materials and Textiles, Zhejiang Sci-Tech University, Hangzhou 310018, China

H.-Y. Yu (✉)
State Key Laboratory for Modification of Chemical Fibers and Polymer Materials, College of Materials Science and Engineering, Donghua University, Shanghai 201620, China
e-mail: phdyu@zstu.edu.cn

Y. Zhou · J.-M. Yao (✉)
National Engineering Lab for Textile Fiber Materials & Processing Technology, Zhejiang Sci-Tech University, Hangzhou 310018, China
e-mail: yaoj@zstu.edu.cn

Introduction

In the recent decades, there are more industrial and agricultural cellulose wastes without re-utilizing, causing many environmental problems such as water pollution, rubbish problem, and haze pollution. Thus these problems should be solved as soon as possible. Recently, a suitable and effective way for reusing these cellulose wastes is to prepare the cellulose nanocrystals (CNCs), because the CNCs act as effective nanoreinforcements in fully biodegradable CNC-reinforced bionanocomposites even at low loading levels, due to their excellent mechanical properties, nanoscale dimension, abundant hydroxyl groups, and

high aspect ratio (Seehra et al. 2014; Yu et al. 2013, 2014a). Therefore, the preparation of CNCs from different industrial and agricultural cellulose materials has attracted considerable interests (Braun and Dorgan 2009; de Morais Teixeira et al. 2010; Lu and Hsieh 2010; Seehra et al. 2014; Tang et al. 2014; Yu et al. 2013).

At present, various methods including sulfuric acid hydrolysis (de Morais Teixeira et al. 2010), 2,2,6,6-tetramethyl-1-piperidiny-loxy mediated oxidation (Li et al. 2015b; Saito et al. 2006), enzymatic hydrolysis combined with mechanical shearing (Pääkkö et al. 2007), steam explosion (Cherian et al. 2008), and enzyme-assisted hydrolysis (Satyamurthy et al. 2011) have been reported for the preparation of CNCs. CNCs can be produced from variety of sources like microcrystalline cellulose (MCC; Yu et al. 2013), *Posidonia oceanica* (Bettaieb et al. 2015), tomato peels (Jiang and Hsieh 2015), and other cellulose raw materials (Cherian et al. 2008; Haafiz et al. 2013; Lu et al. 2015; Martínez-Sanz et al. 2011; Martins et al. 2015; Satyamurthy et al. 2011; Silvério et al. 2013). However, the as-produced CNCs still exhibit low yield for sulfuric acid hydrolysis (yield of 10–30 %, Martins et al. 2015), long preparation period for controlled hydrolysis of the obtained MCCs under anaerobic microbial consortium (at least 7 days, Satyamurthy and Vigneshwaran 2013), and especially only hydroxyl groups or residual sulfate groups (SO_4^{2-}) (Braun and Dorgan 2009; de Morais Teixeira et al. 2010). These disadvantages limit the applications in the high-performance nanocomposites. The low yield and long preparation period will restrict the large scale production of nanocomposites, while the sulfate groups and hydrophilic nature will result in poor thermal stability for simple melt blending and only preparation of water-soluble polymer nanocomposites, respectively. Therefore, a novel route for the simultaneous extraction and functionalization of CNCs from cellulose wastes becomes more and more important. This is beneficial for extraction and functionalization of CNCs, and the environmental protecting.

Braun et al. have reported a simple route to prepare the functionalized CNCs by the mixed acid hydrolysis (acetic/hydrochloric acid and butyric/hydrochloric acid) from cotton linter (Braun and Dorgan 2009). The as-prepared esterified CNCs show good dispersion in organic solvents and can be used as polymer reinforcements. Nevertheless, the covalently bonded acetate and butyrate groups on the CNC surface have no reducibility for anchoring metal nanoparticles. Recently, one-step route has been reported for preparing CNCs with formate groups through formic acid and hydrochloric acid (HCOOH/HCl) hydrolysis of MCC (Yu et al. 2014b). The obtained CNCs can act as a template for the synthesis of nanohybrids (Shin et al. 2007, 2008) or reinforcing materials for nanocomposites (Fortunati et al. 2012; Tan et al. 2015). It is worth noting that the reducibility and reinforcing capability are dependent on the formate groups, crystallinity, and thermal stability of CNCs. However, the preparation conditions are not optimized yet, and especially the yield, microstructure, and properties are not evaluated.

It is well known that the preparation process of CNCs was affected by the reaction temperature, reaction time, and acid-to-cellulose raw material ratio. Among these parameters, the reaction time was believed to be the most important parameter (Fan and Li 2012; Yu et al. 2013). In this work, the reaction time was used as a main parameter to investigate its effect on yield, morphology, chemical and crystal structure, and thermal and hydrophobic properties of obtained CNCs. In addition, this method was used to hydrolyze different industrial and agricultural cellulose raw materials including viscose fibers, ginger fibers, and bamboo fibers. The fabrication of CNC/silver (Ag) nanohybrids was carried out, and the reinforcing effect of CNCs on the polylactic acid (PLA) was also studied.

Materials and methods

Materials

MCC was purchased from Sinopharm Chemical Reagent Co., Ltd. Viscose fibers, bamboo fibers, and ginger fibers were supplied by Shandong SilverHawk Chemical Fiber Co., Ltd. and Jiangnan University. PLA was supplied by Bright China Industrial Co. Ltd. Formic acid (HCOOH), hydrochloric acid (HCl), silver nitrate ($AgNO_3$), and ammonia ($NH_3 \cdot H_2O$) were purchased from Hangzhou Mike Chemical Agents Co. Ltd., China. All the chemicals were of

analytical grade and used as received without further purification.

Preparation and functionalization of cellulose nanocrystals

The process for the preparation and functionalization of CNCs is shown in Fig. 1. The MCC (3.00 g) was added to 150 mL mixed acid solution of 90 % HCOOH/10 % HCl (6 M HCOOH and 6 M HCl). The mixture was heated at 80 °C for different reaction time (2, 3, 4, 5, and 6 h) with strongly mechanical stirring. The CNC suspension was neutralized by $NH_3{\cdot}H_2O$, and then followed by washing repeatedly by centrifugation with deionized water (16,000 rpm at 10 °C for 20 min) until the by-products were removed. Finally, the received products were freeze-dried for 48 h. The five samples were designated as CNC-2h, CNC-3h, CNC-4h, CNC-5h, and CNC-6h corresponding to the reaction time. The yields of CNC correspond to the mass of the obtained dry residue divided by the initial mass of material. It should be noted that all the CNCs were adequately soxhlet extracted with ethanol to remove the adsorbed low molecular weight organic compounds and small molecules (carboxylic ions) of CNCs produced during the hydrolysis process. Moreover, the experiments of zeta potential for the five CNC samples have been redone, and the zeta potential values were around −1.2 to −3.5 mV (Table 1).

Extracting CNCs from viscose fibers, ginger fibers, and bamboo fibers

Extraction of CNCs from viscose fibers, ginger fibers, and bamboo fibers was performed though the same way as the preparation route of CNC-4h. In this experiment, all the cellulose raw materials (5 g each sample) were treated by sodium hydroxide solution (200 mL, 4 %) at 80 °C for 2 h to remove hemicellulose and lignin components of the fibers (Bettaieb et al. 2015). Then the suspension was filtered and washed with distilled water until the suspension reached a constant pH of 7. This process was repeated twice. The delignification of the obtained cellulose was treated with a total alkali charge of 20 % expressed in NaOH (based on w/w o.d. cellulose), an anthraquinone concentration of 0.1 % (w/w with respect to o.d. material) at 160 °C for 120 min (Khristova et al. 2005). The liquor to cellulose ratio was changed and fixed at 10. Finally, the treated cellulose was extensively washed with water until the pH of product was at 7.

Preparation of CNC/Ag nanohybrids and PLA/CNC nanocomposites

The CNC/Ag nanohybrids were prepared through redox reaction between CNC-4h with silver ammonia aqueous solution $[Ag(NH_3)_2(OH)]$ at 80 °C, as previously reported (Yu et al. 2014b). The CNC-4h with relatively hydrophobic formate groups was incorporated into PLA. PLA/CNC nanocomposite films (10 wt% CNC-4h) with the thickness of approximately 20–30 μm were prepared by incorporating well-dispersed CNC suspension in chloroform into PLA solution in chloroform. After being visibly dried, the films were further dried under vacuum.

Characterizations

Field-emission scanning electron microscopy (FE-SEM) was employed to observe the morphology of the different CNCs and fractured morphologies of PLA/CNC nanocomposites at room temperature with an acceleration voltage of 1.0 kV. A drop of dilute suspension was allowed to dry on a silicon slice prior to FE-SEM observation. Transmission electron microscopy (TEM) was carried out using a JEM-2100 electron microscope (JEOL, Japan) at 80 kV. Very small amounts of powdered CNCs were dispersed in distilled water and then negatively stained with 2 % (w/v) ethanol solution of uranyl acetate.

The chemical structure was investigated by FT-IR spectrometer (Nicolet 5700, Thermo Electron Corp., USA) at ambient temperature using KBr disk method. Disks containing 2 mg of sample were scanned in the wavenumber range of 4000–400 cm^{-1} with a resolution of 2 cm^{-1}.

The crystalline nature of CNC powders was characterized for phase identification and crystallite size estimation under an X-ray powder diffractometer (XRD, ARL X'RA, Thermo Electron Corp.) with monochromatic Cu Kα (1.54056 Å) radiation (40 kV, 30 mA) in the 2θ range of 5–80° at a scanning rate of 3°/min. The crystallinity was calculated by the flowing equation (Segal et al. 1959; Li et al. 2015a):

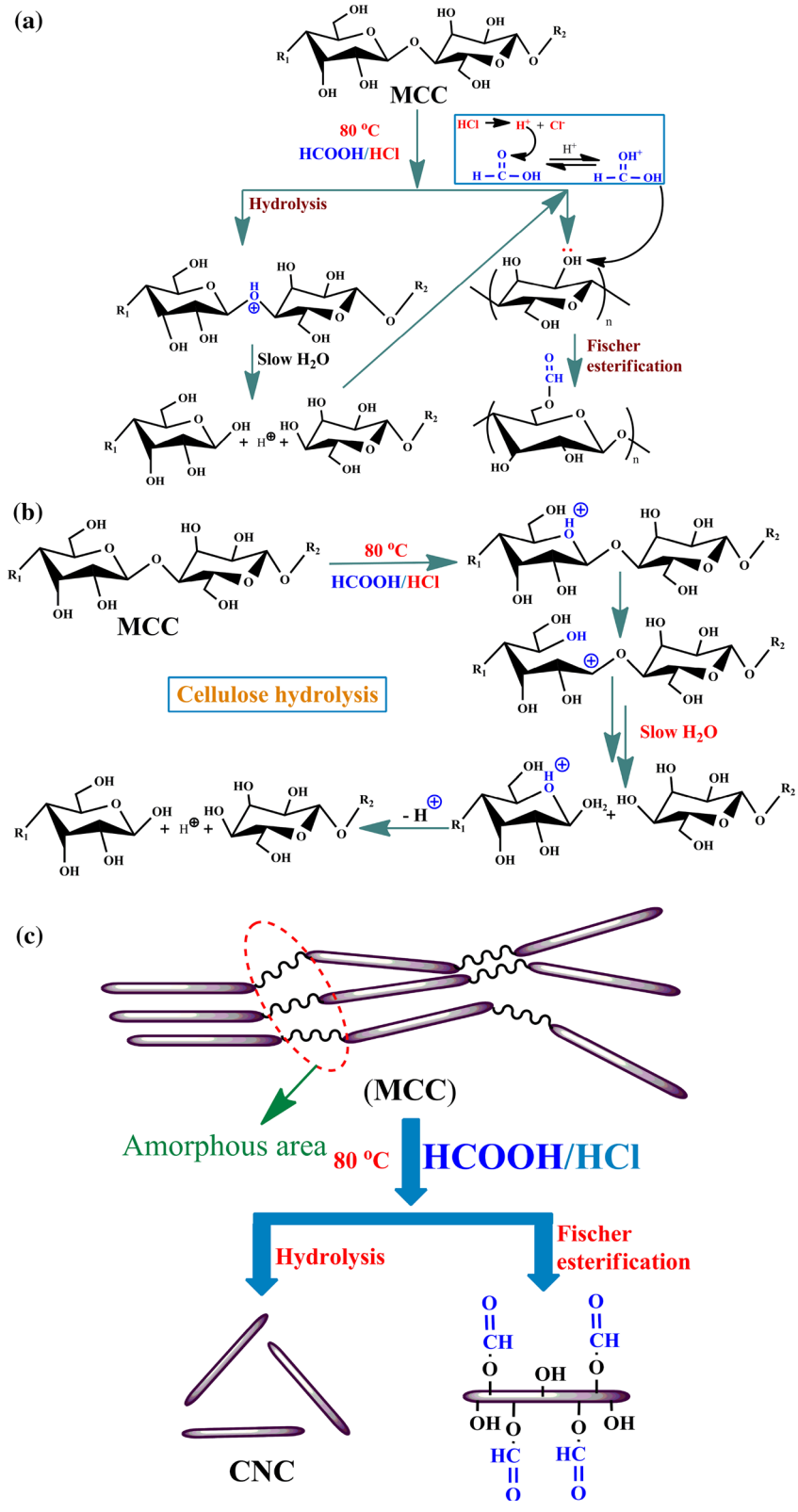

Fig. 1 **a–c** Reaction mechanism of MCC hydrolysis and esterification of hydroxyl groups

Table 1 Length, diameter, aspect ratio, zeta potential value, and formate contents of the CNCs prepared under different reaction time (MCC as raw materials)

Samples	Length[a] (nm)	Diameter[a] (nm)	Aspect ratio	Formate contents[b] (mmol/g)	Zeta potential (mV)
CNC-2h	274.3 ± 51.2	25.8 ± 6.1	11.8 ± 4.8	0.38 ± 0.012	−2.8 ± 0.7
CNC-3h	249.5 ± 59.1	25.4 ± 6.0	10.9 ± 4.9	0.58 ± 0.016	−2.4 ± 0.8
CNC-4h	236.4 ± 40.8	25.6 ± 5.3	9.9 ± 3.6	0.62 ± 0.011	−1.7 ± 0.5
CNC-5h	218.7 ± 46.1	23.6 ± 4.2	9.9 ± 3.7	0.48 ± 0.016	−2.3 ± 0.7
CNC-6h	209.8 ± 38.7	22.9 ± 5.0	9.9 ± 3.8	0.40 ± 0.009	−3.1 ± 0.4

[a] The length and diameter were measured from FE-SEM image

[b] Formate contents were determined by the oxime reaction

$$\text{Crystallinity} = \left[\frac{I_c - I_a}{I_c}\right] \times 100\ \%, \quad (1)$$

where I_c is the peak intensity of crystal plane (200) and I_a is the peak intensity of amorphous phase ($2\theta = 18$–$19°$)

The crystallite sizes of 200, $1\bar{1}0$, and 110 lattice planes were evaluated using the well-known Scherrer equation (Martínez-Sanz et al. 2011):

$$D_{hkl} = \frac{K\lambda}{B_{hkl}\cos\theta}, \quad (2)$$

where D_{hkl} is the crystallite size in the direction normal to the hkl family of lattice planes, $K = 0.94$, λ is the radiation wavelength (1.54 Å), and B_{hkl} is the full width at half-maximum of the peak angle θ of crystal plane.

The thermal stability was conducted using a thermogravimetric analyzer (TGA, Pyris Diamond I, Perkin-Elmer Corporation). The samples with about 8–12 mg were heated from 30 to 600 °C at a heating rate of 20 °C/min under dynamic nitrogen atmosphere with a flow rate of 30 mL/min. The apparent activation energy (E_a) of CNCs was calculated by the Horowitz and Metzger equation (Yu et al. 2014a) from the TGA data:

$$\ln\left[\ln\left(\frac{W_0}{W_T}\right)\right] = \frac{E_a\theta}{RT_s^2}, \quad (3)$$

where W_0 is the starting sample weight, W_T is the residual sample weight at temperature T, θ is value of $T - T_S$, T_S is the temperature determined at 36.43 % weight loss, and R is the gas constant.

The formate group content of CNCs was determined by pH titration through the oxime reaction (Zhang et al. 2014). First, the well-dispersed CNC suspension was fabricated by adding CNC powders (0.1 g) into 30 mL deionized water, and the pH value of the suspension was adjusted to 4.5 by adding dropwisely the hydroxylamine hydrochloride solution (0.43 g in 20 mL deionized water). The resulting mixtures were stirred at room temperature for 24 h. Finally, by titrating 0.01 M NaOH, the mixture reached a constant pH of 4.5, and the formate group content was determined by recording the consumption of NaOH. Each sample was tested three times, and the average value was recorded.

The contact angle was used to evaluate the hydrophobicity of CNCs using SL200B (an equipment for contact angle measurements), USA Kino Industry Co., Ltd. A drop of water (10 μL) was placed on a CNC disk (1.0 cm of diameter, 1 mm of thickness), and the contact angle was determined at the ambient temperature.

The mechanical properties were measured on mechanical testing equipment (Instron 2345) at 20 °C and relative humidity of 65 % with a crosshead speed of 1 mm/min, after equilibration under a controlled environment for at least 24 h. Dumbbell-shaped samples were used (4 × 50 mm^2, 20–30 μm in thickness). Five replicates were tested for each sample.

The optical properties of PLA and PLA/CNC were tested by the UV–vis spectrophotometer (Lambda 35, Perkin-Elmer Corporation, USA) in the wavelength interval between 300 and 1000 nm.

Results and discussion

Preparation and functionalization of cellulose nanocrystal

Figure 1 gives the mechanism of preparation and modification of CNCs through mixed acid hydrolysis

of MCC. The hydronium ions from HCl have two different impacts on the MCC. The H^+ from HCl rapidly protonated the glycosidic oxygen in the hydrolysis process, and the glycosidic bonds are subsequently splitted with the existence of H_2O as shown in Fig. 1a. In this process, the cellulose will be cut into two fragments with the shorter chains, meanwhile they preserve the basic backbone of cellulose (Lu and Hsieh 2010). Another possible mechanism of CNC hydrolysis is shown in Fig. 1b. First, the H^+ from HCl rapidly protonates the ring oxygen during the hydrolysis process, and then leads to the formation of a protonated hemiacetal subsequent to the ring-opening heterolysis. Finally, the glycosidic bonds are also splitted in the presence of H_2O (Klemm et al. 2012). On the other hand, the hydronium ions catalyze the esterification of hydroxyl groups with the carboxyl groups of formic acid. Figure 1c shows the mechanism of hydrolysis and modification at macro level. In the hydrolysis process, the acid can diffuse into the amorphous area of MCC, since the amorphous regions are more accessible to the acid and easily effected by the hydrolytic actions (Lu and Hsieh 2010; Yu et al. 2013), compared to the crystalline regions. As a result, more crystalline regions will be remained and more amorphous regions will be hydrolyzed, leading to an increase in the crystallinity. Simultaneously, Fischer esterification with the hydroxyl groups on the exposed cellulose chains can generate the formates on the CNCs. In general, the formate groups increase with the deepening of esterification reaction (the reaction time below 4 h). However, the decreasing of formate groups is caused by the acid hydrolysis of the esterified part of cellulose, because the esterification reaction occurs in the amorphous regions of cellulose. These two opposite effects could result in the content of formate groups achieving the maximum at an extent of reaction (in this work, the formate groups reached the maximum at 4 h), which was supported by the determination of formate group contents (Table 1). The CNC samples have different formate contents of 0.38, 0.58, 0.62, 0.48, and 0.40 mmol/g, and CNC-4h indeed shows the highest formate content value.

Figure S1a shows the CNC yield of CNCs prepared under different reaction time. With an increase of reaction time, the yield of CNCs was first increased a maximum value at 4 h, and then decreased. It suggests that the long reaction time will further hydrolyze some small size CNCs, causing the reduction in CNC yield. Figure S1b gives the CNC yield of the CNCs extracted from viscose fibers, ginger fibers, and bamboo fibers. The relatively high CNC yield of 70–90 % was kept (Martins et al. 2015).

Morphological analysis of CNCs

Figure 2 shows the morphologies of MCC and CNCs, the measurements of diameter and length of CNCs are listed in Table 1. Before hydrolysis, MCC exhibited the curled fibrils with the width in the range of 10–40 μm. After the hydrolysis of MCC, the microfibrils in the original cellulose were swollen and separated into much smaller rod-like CNCs, which were same as the previous reports (Jiang and Hsieh 2015; Lazko et al. 2014). For the FE-SEM images, we choose 100 amounts of CNCs to calculate the average length and diameter of CNCs, and the size distribution histograms for length and diameter were shown in Figs. S2 and S3. The length of 274.3, 249.5, 236.4, 218.7, and 209.8 nm with the diameter of 25.8, 25.4, 25.6, 23.6, and 22.9 were observed for CNC-2h, CNC-3h, CNC-4h, CNC-5h, and CNC-6h, respectively. Furthermore, the TEM images (Fig. S4) of CNC-2h, CNC-4h, and CNC-6h showed the lengths were 267.1, 230.5, and 206.4 nm. This result was consistent with change trend of FE-SEM results. And the diameters calculated from TEM were 10.7, 10.2, and 9.3 nm (Table S1) for CNC-2h, CNC-4h, and CNC-6h, respectively. This result was in agreement with the CNCs reported by Elazzouzi-Hafraoui et al. (2008). The results confirmed the assumption that the CNCs can be successfully prepared by one-step mixed acid hydrolysis of MCC. Furthermore, with the increase of reaction time, both the length and diameter of CNCs were gradually decreased, indicating that the amorphous regions of CNC nanorods were hydrolyzed by the acids.

Figure 3 shows the FE-SEM images of three other cellulose raw materials including bamboo fiber, ginger fiber, and viscose fiber (a, c, e) and resulting CNCs (b, d, f). In Fig. 3a, c, e, bamboo fiber and ginger fiber exhibited lumpy granules, while viscose fiber showed obvious fiber shape. After acid hydrolysis, in Fig. 3b, d, the CNCs (obtained from bamboo fiber and ginger fiber) showed a slender and nanofibrillated shape with average width was 30 nm and the length of 1 μm. Figure 3f shows the spherical CNCs (from viscose fiber) with the width of 56 nm. It can be concluded that this simple

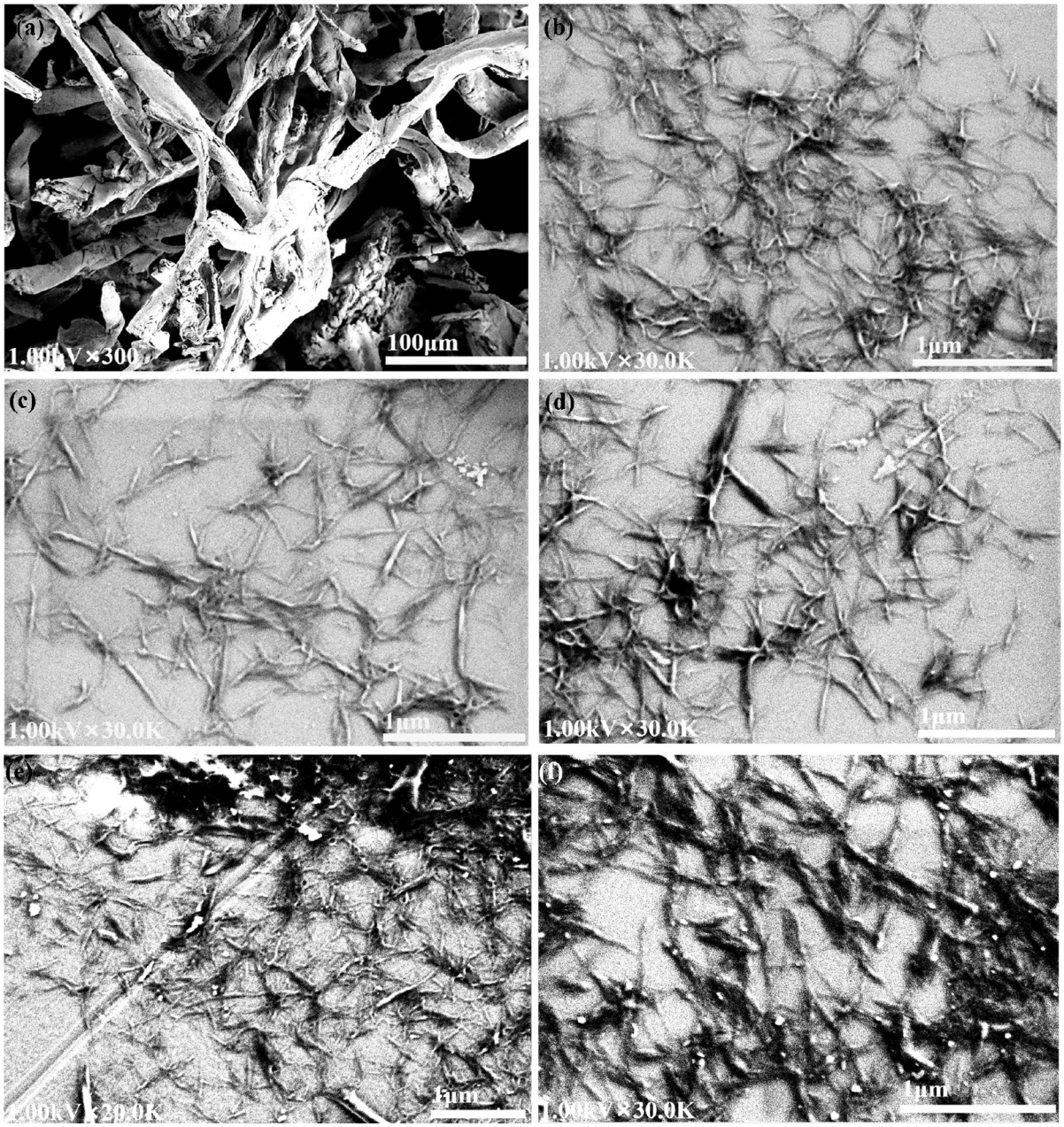

Fig. 2 FE-SEM images of **a** MCC, **b** CNC-2h, **c** CNC-3h, **d** CNC-4h, **e** CNC-5h, and **f** CNC-6h

route was also universal for hydrolyzing other different industrial and agricultural cellulose materials.

Chemical structure of MCC and CNCs

Figure 4a shows the FT-IR spectra of MCC and CNCs. For MCC and CNC samples, a strong band at the region of 3600–3000 cm^{-1} was assigned to O–H stretching vibration, peaks at 2900, 1637, 1374, and 1060 cm^{-1} can be related to the aliphatic saturated C–H stretching vibration, the O–H bending of the absorbed water, the C–H deformation vibration, and the C–O–C stretching of pyranose, respectively (Altaner et al. 2014; Lu and Hsieh 2010; Yu et al. 2013).

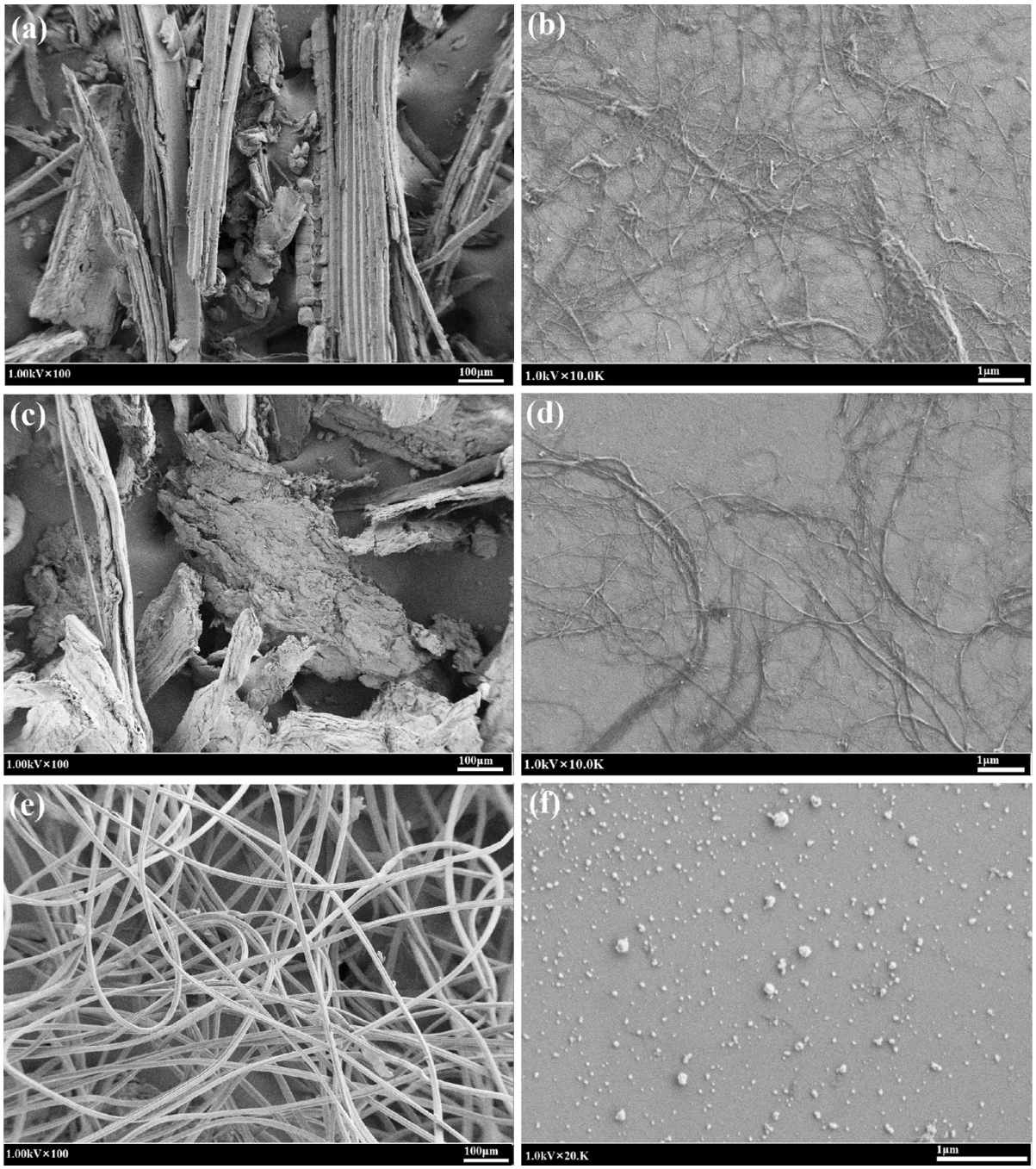

Fig. 3 FE-SEM images of **a** bamboo fiber, **b** CNCs (bamboo fiber), **c** ginger fiber, **d** CNCs (ginger fiber), **e** viscose fiber, and **f** CNCs (viscose fiber)

Both of the MCC and CNCs were belonged to the cellulose Iβ, because the crystalline Iβ characteristic peaks are present at: O–H stretching at 3270 cm^{-1} and O–H out-of-plane bending at 710 cm^{-1} (Lu and Hsieh 2010; Yu et al. 2013). This result was consist with the diffraction patterns of MCC and CNCs (Fig. S5), which exhibited the typical monoclinic cellulose I at $2\theta = 14.6°$, 16.5°, and 22.6° corresponding to the $1\bar{1}0$,

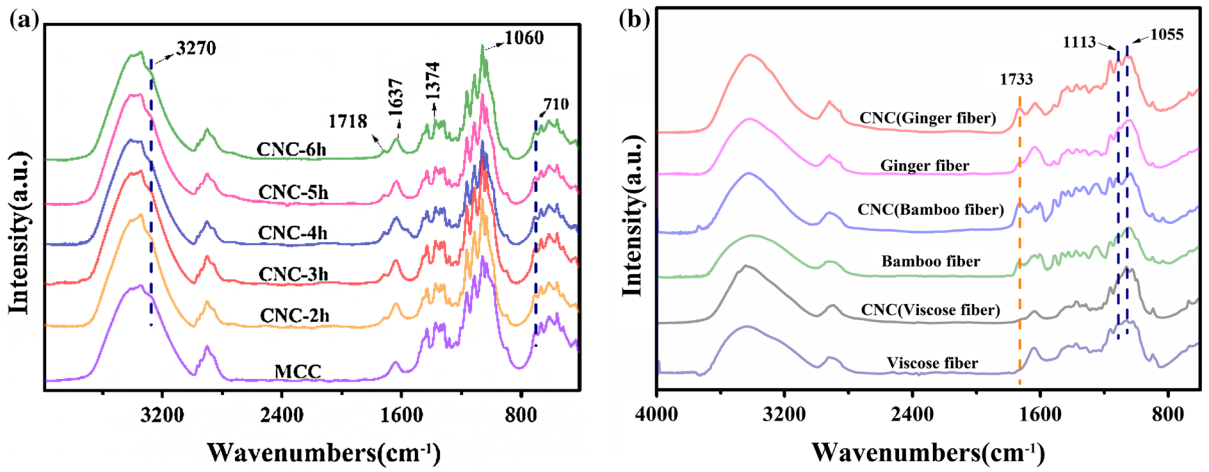

Fig. 4 **a** FT-IR spectra of MCC and CNCs, and **b** FT-IR spectra of CNCs extract from (bamboo fiber, ginger fiber, and viscose fiber)

110, and 200 crystallographic planes (Lazko et al. 2014; Wang et al. 2007). These peaks match well for all the spectra and no significant difference is found, suggesting no change in chemical structure of CNCs after the acid hydrolysis. Furthermore, compared with the original MCC, the obtained CNCs with formate groups presented a new C=O stretching peak at 1718 cm^{-1}. In Fig. S6a, a similar peak at 1736 cm^{-1} was found for C=O groups (from ester groups) of CNCs prepared by acetic acid and hydrochloric acid hydrolysis of MCC. This result can confirm that both the hydrolysis and esterification of hydroxyl groups can were successful performed by above mixed acid. In addition, the normalized intensity of C=O and the formate contents are given in Fig. S7. It is found that the normalized intensity of C=O was increased to a maximum at the reaction time of 4 h, and then decreased. This was consistent with the change tendency of formate group contents, suggesting that the preparation and modification processes were successfully carried out.

Figure 4b shows the FT-IR spectra of the three different cellulose material and the resulting CNCs. Compared to the viscose fiber, a new peak at 1733 cm^{-1} appeared in the FT-IR spectra of CNC (viscose fiber), suggesting that the formate groups were successfully grafted on the CNC surface. The increased intensities of the peak at 1733 cm^{-1} were found for the other CNCs (extracted from bamboo fiber and ginger fiber), since the weak band at 1733 cm^{-1} was assigned to other components for original bamboo fiber and ginger fiber. Furthermore, all the spectra of CNC exhibited increased intensities for the bands at 1055 and 1113 cm^{-1} that assigned to the C–O–C stretching of pyranose and glycose ring skeletal vibration, respectively. It hints the increase in crystalline cellulose contents for the CNC samples (Yu et al. 2013).

Thermal stability of MCC and CNCs

The thermal behavior of CNCs could significantly affect the application of CNCs as the reinforcing material for thermoprocessed nanocomposites. The thermal behavior of MCC and CNCs was investigated through TGA, and the thermal degradation onset temperature (T_0) and maximum degradation temperature (T_{max}) are listed in Table S2. Generally, the thermal degradation of cellulose involves depolymerization, dehydration, and decomposition of glycosyl units followed by formation of a charred residue (Yu et al. 2014a). Figure 5a, b shows the TGA and DTG curves of MCC and CNCs. The TGA results illustrated that compared with MCC, the degradation curves of CNCs were shifted to higher temperature, indicating an enhancement in the thermal stability of CNCs due to the increased crystallinity and reduction of thermally unstable hydroxyl groups. Furthermore, the CNC-4h had the highest thermal stability, and the T_0 and T_{max} were increased from 298.5 and 352.7 °C (MCC) to 333.1 and 383.0 °C, respectively. This can be explained by the fact that CNC-4h had the higher

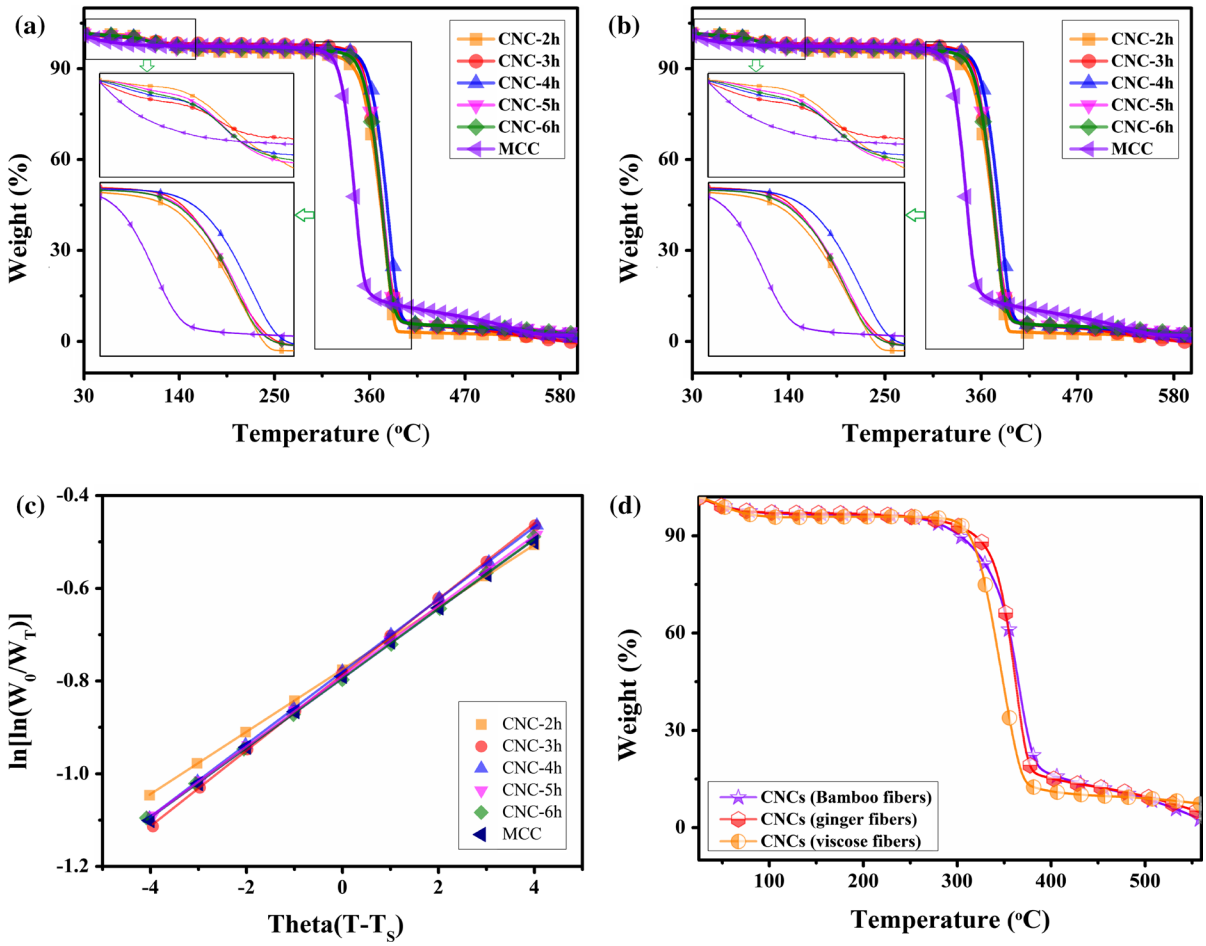

Fig. 5 **a** TGA, **b** DTG curves, **c** plot of $\ln[\ln(W_0/W_T)]$ versus θ of MCC and CNCs, and **d** TGA curves of CNCs extract from (bamboo fiber, ginger fiber, and viscose fiber)

crystallinity and more formate groups. In addition, the maximum degradation temperature of CNC-4h was higher than that of CNCs prepared by H_2SO_4 or H_2SO_4/HCl mixed acid hydrolysis from MCC (253.2 °C, Yu et al. 2013), MCC (339 °C, Wang et al. 2007), phosphoric acid hydrolysis of filter paper (325 °C, Camarero Espinosa et al. 2013), and acetic and hydrochloric acid hydrolysis of MCC (338.5 °C, Fig. S6b) under the heating rate of 20 °C/min. Figure 5c shows the plot of $\ln[\ln(W_0/W_T)]$ versus θ for the main stage of the thermal degradation of MCC and CNCs. The average apparent activation energy (E_a) can be calculated from the slope of fit lines using Horowitz and Metzger method and lists in Table S2. Generally, the higher E_a represents a faster degradation rate (Yu et al. 2014a). Table S2 illustrates that CNC-3h and CNC-4h had the larger E_a than those of MCC and other CNCs. Both higher crystallinity and formate group contents enhanced their thermal degradation temperature so that the onset of the thermal degradation temperature of CNC-3h and CNC-4h occurred at a higher temperature, resulting in the increased degradation rate for both samples.

Figure 5d shown the TGA a curves of CNCs obtained from three other cellulose raw materials. The results of TGA curves showed that the different CNCs have different thermal degradation temperature due to various raw materials. For example, the T_0 of the CNCs were 271.5 °C (bamboo fibers), 279.6 °C (ginger fibers), and 291.4 °C (viscose fiber), while T_{max} of the CNCs were 388.2 °C (bamboo fibers), 382.7 °C (ginger fibers), and 368.9 °C (viscose fiber),

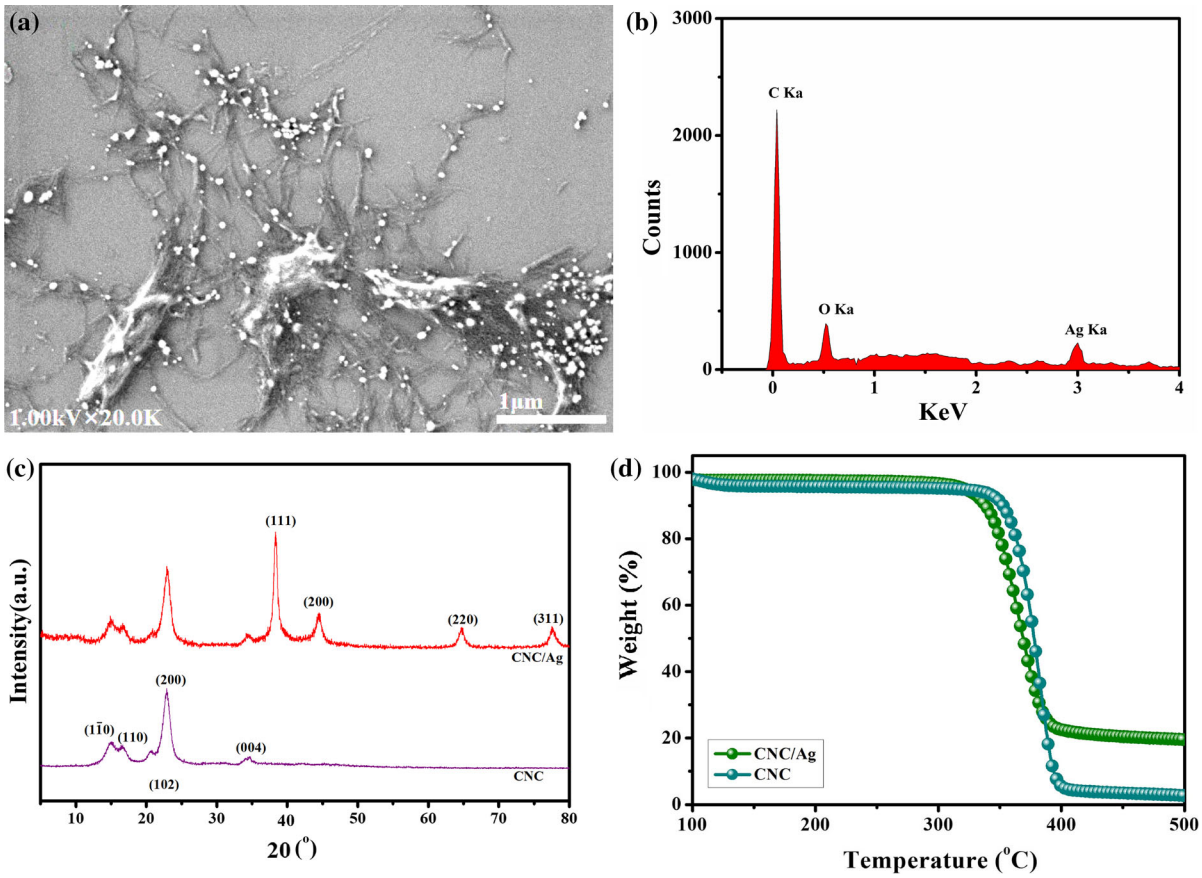

Fig. 6 **a** FE-SEM images, **b** EDS of CNC/Ag nanohybrids, **c** XRD spectra and **d** TGA curves of CNC and CNC/Ag nanohybrids

respectively. In this work, the T_{max} of the CNCs (bamboo fibers) was higher than that of bamboo CNCs prepared by the phosphoric acid hydrolysis (350 °C, Lu et al. 2015). The T_{max} of the CNCs (ginger fibers) was higher than that of the bleached ginger (360 °C, Zaki et al. 2014). And the T_{max} of the CNCs (viscose fiber) was similar as that of SCNFs (365.4 °C, Yan et al. 2015). These confirmed that the CNCs with high thermal stability was extracted successfully from three different cellulose raw materials by simple route.

Potential applications

Template for anchoring metal nanoparticles

Generally, the CNC/Ag nanohybrids can be used as the bifunctional reinforcements in the nanocomposites (Xu et al. 2013; Yu et al. 2014c). Thus the CNCs with the formate groups were used as an effective template for synthesis of CNC/Ag nanohybrids. Since the CNCs have many formate groups with the reducibility, the CNC/Ag nanohybrids were synthesized by reaction between CNCs and silver–ammonia solution. Figure 6a, b shows the FE-SEM images and EDS of CNC/Ag nanohybrids, confirming the successful synthesis of the CNC/Ag nanohybrids. Furthermore, Fig. 6c shows the XRD spectra of CNC and CNC/Ag nanohybrids. The peaks at 14.6°, 16.5°, 22.6°, and 34.5° were associated to (1$\bar{1}$0), (110), (200), and (004) planes of cellulose Iβ, respectively while the peaks at 38.4° and 44.5° were attributed to (111), (200) crystallographic planes of cubic Ag^0 nanoparticles, respectively (Yu et al. 2014b). Figure 6d shows the thermal stability of CNC and CNC/Ag nanohybrid. The CNC/Ag nanohybrid shows a relatively high T_{max} value (368.6 °C), which was higher than that of the similar cellulose/Ag hybrids prepared using fructose and glucose by hydrothermal method (T_{max} of 307 °C, Dong et al. 2014) due to the strong interaction between CNC and Ag nanoparticles. The reduction reaction

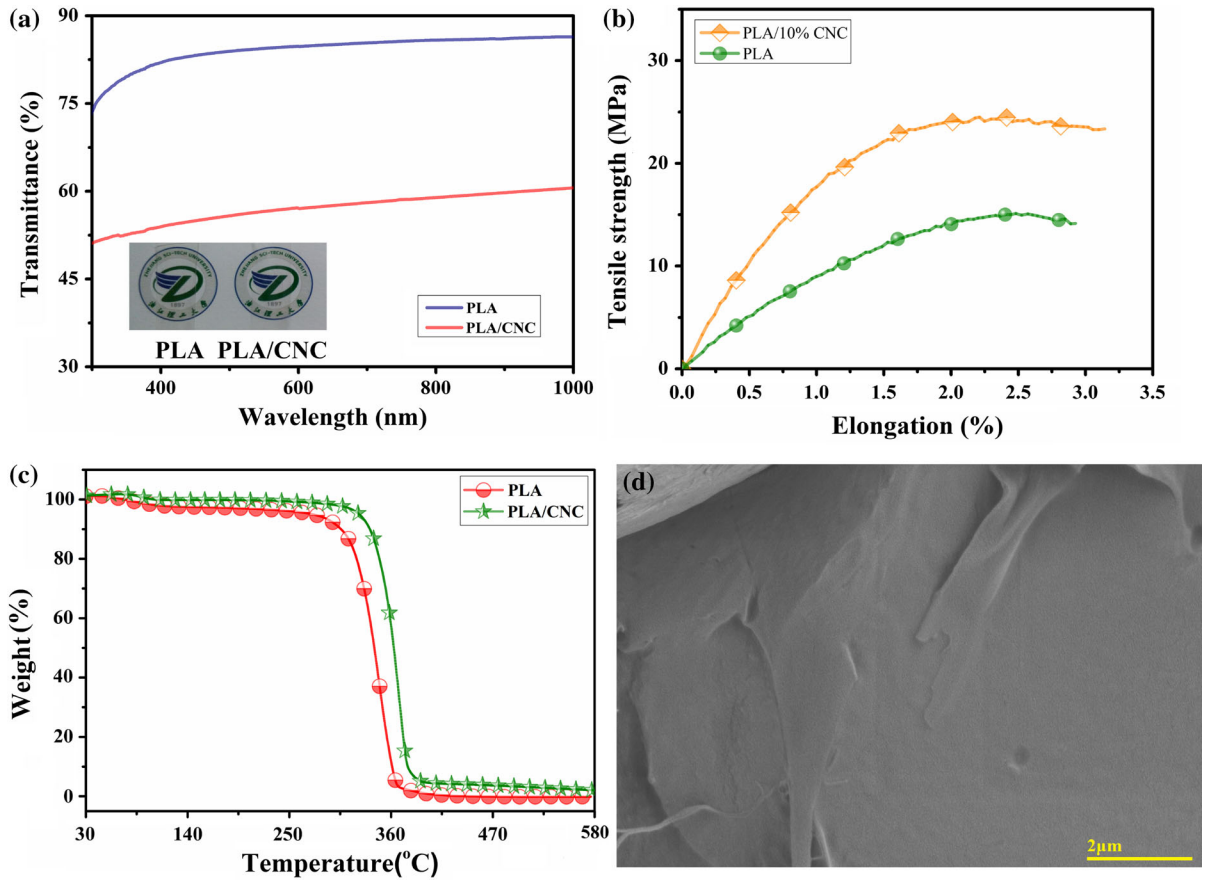

Fig. 7 **a** UV–vis transmittance spectra and visual observation (*inset photos*), **b** stress–strain curves, **c** TGA curves of neat PLA and PLA/CNC nanocomposite, and **d** FE-SEM image for fracture morphologies of PLA/CNC nanocomposite

equation between CNC and $Ag(NH_3)_2OH$ was shown as below:

$$\text{R-CHO} + 2\text{Ag}(\text{NH}_3)_2\text{OH} \rightarrow \text{R-CHOONH}_4 + 2\text{Ag} + 3\text{NH}_3 + \text{H}_2\text{O}.$$

The amount of Ag nanoparticle could be calculated by follows:

$$m_{\text{Ag}} = \frac{C_{\text{F}} \times m_{\text{CNC}} \times 2 \times 108}{1000}, \quad (4)$$

where C_{F} was the formate group content (mmol/g) of CNC, m_{CNC} was the mass (g) of the CNC, and 108 g/mol was the molar mass of the Ag.

Reinforcing material in the nanocomposites

The CNCs with relatively hydrophobic formate groups were incorporated into PLA (as a mode biopolymer) to evaluate their reinforcing efficiency. From Fig. 7a, PLA/CNC showed a decreased transparency from 86 % (neat PLA) to 60 % at 800 nm, but still possessed good transparency (see the picture inset in Fig. 7a). The mechanical results show that tensile strength of PLA/CNC nanocomposite was significantly improved by 63.3 % compared with pure PLA (Fig. 7b). Also, the TGA result showed an improved thermal stability in PLA/CNC nanocomposite (Fig. 7c). The T_{max} was improved from 342.1 °C for neat PLA to 363.3 °C for the nanocomposite. Furthermore, the fractured FE-SEM images of the nanocomposites illustrated no any obvious two-phase separation (Fig. 7d), indicating good dispersion/compatibility between the PLA matrix and the CNCs with formate groups. It confirmed that the CNCs with hydrophobic formate groups may improve the interfacial interaction between two components, and thus

significantly enhanced the mechanical strength and thermal stability of biopolymers.

Conclusions

In summary, the rod-like CNCs, nanofibrillated CNCs, and spherical CNCs with formate groups were successfully fabricated by simple HCOOH/HCl hydrolysis of MCC, ginger fiber, bamboo fiber, and viscose fiber, respectively. Under the optimal hydrolysis time of 4 h, the CNC-4h (MCC) with the highest formate contents had the improved crystallinity and thermal stability. In addition, it was confirmed that this route was suitable for the extraction of CNCs from other cellulose raw materials. Moreover, the CNC/Ag nanohybrids were successfully synthesized using the reducibility of formate groups on the CNC surface. Further, the CNCs have strong reinforcing efficiency on the PLA matrix.

Acknowledgments This work was funded by State Key Laboratory for Modification of Chemical Fibers and Polymer Materials, Donghua University (LK1428), The National Natural Science Foundation of China (51403187), The Public Technology Research Plan of Zhejiang Province, China, under Grant No. 2015C33111, Zhejiang Provincial Natural Science Foundation of China under Grant No. LQ14E030007, "521" Talent Project of Zhejiang Sci-Tech University, and Open Fund in Top Priority Discipline of Zhejiang Province in Zhejiang Sci-Tech University (2015YXQN04, 2015YXQN11).

References

Altaner CM et al (2014) Cellulose Iβ investigated by IR-spectroscopy at low temperatures. Cellulose 21:3171–3179

Bettaieb F et al (2015) Preparation and characterization of new cellulose nanocrystals from marine biomass Posidonia oceanica. Ind Crops Prod 72:175–182

Braun B, Dorgan JR (2009) Single-step method for the isolation and surface functionalization of cellulosic nanowhiskers. Biomacromolecules 10(2):334–341

Camarero Espinosa S et al (2013) Isolation of thermally stable cellulose nanocrystals by phosphoric acid hydrolysis. Biomacromolecules 14(4):1223–1230

Cherian BM et al (2008) A novel method for the synthesis of cellulose nanofibril whiskers from banana fibers and characterization. J Agric Food Chem 56(14):5617–5627

de Morais Teixeira E et al (2010) Cellulose nanofibers from white and naturally colored cotton fibers. Cellulose 17(3):595–606

Dong YY et al (2014) Compare study cellulose/Ag hybrids using fructose and glucose as reducing reagents by hydrothermal method. Carbohydr Polym 106:14–21

Elazzouzi-Hafraoui S et al (2008) The shape and size distribution of crystalline nanoparticles prepared by acid hydrolysis of native cellulose. Biomacromolecules 9(1):57–65

Fan JS, Li YH (2012) Maximizing the yield of nanocrystalline cellulose from cotton pulp fiber. Carbohydr Polym 88(4):1184–1188

Fortunati E et al (2012) Effects of modified cellulose nanocrystals on the barrier and migration properties of PLA nanobiocomposites. Carbohydr Polym 90(2):948–956

Haafiz MM et al (2013) Physicochemical characterization of cellulose nanowhiskers extracted from oil palm biomass microcrystalline cellulose. Mater Lett 113:87–89

Jiang F, Hsieh YL (2015) Cellulose nanocrystal isolation from tomato peels and assembled nanofibers. Carbohydr Polym 122:60–68

Khristova P, Kordsachia O, Khider T (2005) Alkaline pulping with additives of date palm rachis and leaves from Sudan. Bioresour Technol 96(1):79–85

Klemm D et al (2012) Fundamentals and analytical methods. In: Klemm D, Heinze T, Heinze U, Edgar KJ, Philipp B, Zugenmaier P (eds) Comprehensive cellulose chemistry. Wiley-VCH, Weinheim, pp 83–85

Lazko J et al (2014) Well defined thermostable cellulose nanocrystals via two-step ionic liquid swelling-hydrolysis extraction. Cellulose 21(6):4195–4207

Li MC et al (2015a) Cellulose nanoparticles: structure–morphology–rheology relationships. ACS Sustain Chem Eng 3(5):821–832

Li MC et al (2015b) Cellulose nanoparticles as modifiers for rheology and fluid loss in bentonite water-based fluids. ACS Appl Mater Interfaces 7(8):5006–5016

Lu P, Hsieh YL (2010) Preparation and properties of cellulose nanocrystals: rods, spheres, and network. Carbohydr Polym 82(2):329–336

Lu Q et al (2015) A mechanochemical approach to manufacturing bamboo cellulose nanocrystals. J Mater Sci 50(2):611–619

Martínez-Sanz M, Lopez-Rubio A, Lagaron JM (2011) Optimization of the nanofabrication by acid hydrolysis of bacterial cellulose nanowhiskers. Carbohydr Polym 85(1):228–236

Martins DF et al (2015) The influence of the cellulose hydrolysis process on the structure of cellulose nanocrystals extracted from capim mombaça (*Panicum maximum*). Ind Crops Prod 65:496–505

Pääkkö M et al (2007) Enzymatic hydrolysis combined with mechanical shearing and high-pressure homogenization for nanoscale cellulose fibrils and strong gels. Biomacromolecules 8(6):1934–1941

Saito T et al (2006) Homogeneous suspensions of individualized microfibrils from TEMPO-catalyzed oxidation of native cellulose. Biomacromolecules 7(6):1687–1691

Satyamurthy P, Vigneshwaran N (2013) A novel process for synthesis of spherical nanocellulose by controlled hydrolysis of microcrystalline cellulose using anaerobic microbial consortium. Enzyme Microb Technol 52(1):20–25

Satyamurthy P et al (2011) Preparation and characterization of cellulose nanowhiskers from cotton fibres by controlled microbial hydrolysis. Carbohydr Polym 83(1):122–129

Seehra MS et al (2014) Hydrothermal treatment of microcrystalline cellulose under mild conditions: characterization of solid and liquid-phase products. Cellulose 21(6):4483–4495

Segal L et al (1959) An empirical method for estimating the degree of crystallinity of native cellulose using the X-ray diffractometer. Text Res J 29(10):786–794

Shin Y et al (2007) Simple preparation and stabilization of nickel nanocrystals on cellulose nanocrystal. Mater Lett 61(14):3215–3217

Shin Y et al (2008) Facile stabilization of gold–silver alloy nanoparticles on cellulose nanocrystal. J Phys Chem C 112(13):4844–4848

Silvério HA et al (2013) Extraction and characterization of cellulose nanocrystals from corncob for application as reinforcing agent in nanocomposites. Ind Crops Prod 44:427–436

Tan C et al (2015) Role of surface modification and mechanical orientation on property enhancement of cellulose nanocrystals/polymer nanocomposites. Eur Polym J 62:186–197

Tang Y et al (2014) Preparation and characterization of nanocrystalline cellulose via low-intensity ultrasonic-assisted sulfuric acid hydrolysis. Cellulose 21(1):335–346

Wang N, Ding E, Cheng R (2007) Thermal degradation behaviors of spherical cellulose nanocrystals with sulfate groups. Polymer 48(12):3486–3493

Xu X et al (2013) Properties of novel polyvinyl alcohol/cellulose nanocrystals/silver nanoparticles blend membranes. Carbohydr Polym 98(2):1573–1577

Yan CF, Yu HY, Yao JM (2015) One-step extraction and functionalization of cellulose nanospheres from lyocell fibers with cellulose II crystal structure. Cellulose 22(6):3773–3788

Yu H et al (2013) Facile extraction of thermally stable cellulose nanocrystals with a high yield of 93% through hydrochloric acid hydrolysis under hydrothermal conditions. J Mater Chem A 1(12):3938–3944

Yu H et al (2014a) Reinforcement of biodegradable poly(3-hydroxybutyrate-*co*-3-hydroxyvalerate) with cellulose nanocrystal/silver nanohybrids as bifunctional nanofillers. J Mater Chem B 2(48):8479–8489

Yu H, Yan C, Yao J (2014b) Fully biodegradable food packaging materials based on functionalized cellulose nanocrystals/poly(3-hydroxybutyrate-*co*-3-hydroxyvalerate) nanocomposites. RSC Adv 4(104):59792–59802

Yu HY et al (2014c) A facile one-pot route for preparing cellulose nanocrystal/zinc oxide nanohybrids with high antibacterial and photocatalytic activity. Cellulose 22:261–273

Zaki FA, Abdullah I, Ahmad I (2014) The physical and chemical natures of cellulose extracted from torch ginger stems. Int J Mater Eng Innov 5(1):48–60

Zhang X et al (2014) Direct immobilization of antibodies on dialdehyde cellulose film for convenient construction of an electrochemical immunosensor. Sens Actuator B 200:304–309